12th International Symposium on Turbulence and Shear Flow Phenomena (TSFP12)
Osaka, Japan (Online), July 19-22, 2022

INFLOW TURBULENCE GENERATION USING EQUIVALENT BOUNDARY LAYER

Haining Wang
Department of Engineering Mechanics
Tsinghua University
Haidian District, Beijing, 100084, P. R. China
whn17@mails.tsinghua.edu.cn

Weixi Huang
Department of Engineering Mechanics
Tsinghua University
Haidian District, Beijing, 100084, P. R. China
hwx@tsinghua.edu.cn

Chunxiao Xu
Department of Engineering Mechanics
Tsinghua University
Haidian District, Beijing, 100084, P. R. China
xucx@tsinghua.edu.cn

ABSTRACT

Eddy-resolved simulation of external flow usually requires inflow conditions representing a zero-pressure-gradient turbulent boundary layer (ZPGTBL) flow, and the quality of the inflow conditions directly impact the accuracy of the simulation. The present study proposes a new method to generate ZPGTBL-type inflow turbulence, i.e. the equivalent boundary layer (EBL). Based on half channel model, EBL approximates ZPGTBL flow by recovering the mean momentum balance with driving force. It simulates streamwise equilibrium turbulence, applying periodic boundary conditions, and thus overcomes the complexity and artificiality incurred by the classic recycling-rescaling methods. The current paper discusses the difference between turbulent channel and boundary layer flows from the equation point of view, and designs the driving force corresponding to the mean inertial force of boundary layer. Also, the total shear stress models for obtaining the driving force are validated both *a priori* and *a posteriori*. Direct numerical simulations (DNS) are carried out for EBLs at $Re_\theta = 1000, 1420$ and 2000 (where Re_θ is the Reynolds number based on momentum thickness), showing that EBL well reflects the statistical characteristics of ZPGTBL at corresponding Reynolds numbers. The application of EBL to the generation of inflow conditions is also demonstrated by DNS of turbulent boundary layers with inlet $Re_\theta = 1000, 1420$ and 2000. The computational results agree well with generally acknowledged DNS data published in literature, in terms of streamwise developing statistics and profiles and energy spectra at characteristic cross-sections. Judging from the mean velocity, the adjustment section is shorter than one boundary layer thickness.

1 INTRODUCTION

The present study focuses on the generation of inflow turbulence fluctuations representing the zero-pressure-gradient turbulent boundary layer (TBL). A classic approach to this goal is the 'LWS' method, proposed by Lund *et al.* (1998) and adapted from the coordinate transformation method by Spalart (1988). Due to its simplicity and low cost in computation, LWS method has been one of the most popular methods in inflow turbulence generation. The basic idea of LWS method is to rescale the downstream flow based the self-similarity of TBL and reintroduce it to the inlet. Its key assumption is that the inner region of TBL flow scales in y^+ and the outer region in y/δ, where y^+ and y/δ are the wall-normal coordinates measured by inner and outer length scales respectively. Therefore, after piecewise rescaling and appropriate matching, flow at a downstream position can be recycled to serve as boundary condition at the inlet.

Despite the major success achieved, LWS method is subject to some drawbacks. The method is artificial in three respects. 1. It relies on the streamwise developing law of TBL, which is derived from the log law or power law of the mean velocity. 2. It explicitly assumes the form of self-similarity, including the universal law of the wall in the inner region and defect law in the outer region, which, though being fairly precise for the mean streamwise velocity, are not satisfactory for the mean wall-normal velocity and velocity fluctuations; Moreover, the range of applicability of these two laws are not precisely clear, which leads to the third problem: 3. The weighting function and its parameters to match the two regions are empirically chosen, reflecting the arbitrariness in applying the inner and outer laws. Another difficulty concerns the choice of the recycling position. The recycling plane should not be too close to the inlet, because it must fall in healthy flow sections possessing self-similarity, avoiding unphysical adjustment zones near the inlet and outlet; Besides, sufficient natural evolution of turbulence structures should be accommodated between the inlet and recycling plane, especially for high-Reynolds-number turbulence which contains abundant large-scale structures. On the other hand, the recycling plane should not be too far from the inlet, because the spanwise and temporal scales need also be matched aside from the wall-normal rescaling.

The above discussion has revealed the shortcomings of the traditional method in generating TBL-type inflow turbulence. In the current study, we propose a new method to generate TBL-type inflow turbulence fluctuations. This method is based on the open-channel model, therefore naturally applying the streamwise periodic boundary condition to simulation of the spatially homogeneous flow. Meanwhile, in order to fill the gap between channel flow and TBL, external force is added to the open-channel flow to drive it closer to the real TBL. The rest of the paper is organized as follows. In Section 2 we introduce the mathematical formulations including the theoretic basis of EBL and how the driving force can be modelled. In Section 3 the idea of using EBL to generate inflow turbulence for TBL is validated by DNS *a priori* and *a posteriori*. Finally, in Section 4, we conclude the present work.

2 FORMULATION

The computational models in the current study are open-channel and TBL, whose symbols and notations are defined as follows. x, y, z represent the streamwise, wall-normal and spanwise directions respectively, and u, v, w are the corresponding velocity components (also denoted by their vector forms $\boldsymbol{x}, \boldsymbol{u}$). The boundary layer thickness, displacement thickness and momentum thickness are denoted by δ, δ^*, θ respectively. The Reynolds number $Re = U_\infty \delta / \nu$ is defined by the boundary layer thickness, free velocity U_∞ and kinetic viscosity ν. Also frequently used are the Reynolds number based on the momentum thickness $Re_\theta = U_\infty \theta / \nu$ and the friction Reynolds number $Re_\tau = u_\tau \delta / \nu$, where u_τ is the friction velocity. The superscript '+' represents normalization by the wall viscous units, and $\eta = y/\delta$ is the wall-normal coordinate scaled by outer boundary layer thickness. The prime symbol '$(\cdot)'$' represents fluctuations and the angle bracket '$\langle \cdot \rangle$' or capital letters represent mean quantities averaged along temporal and spanwise (and streamwise if the flow is streamwise equilibrium) directions.

2.1 EQUIVALENT BOUNDARY LAYER

Existing researches have explained the difference between channel and TBL flows from the aspect of physical mechanisms. Here we try to look for another interpretation from the equation point of view. The theory of turbulence energy hierarchy has made clear that the energy is first extracted from the mean motion, transferred from large to small scales, and eventually transformed into heat at dissipation scales. Therefore, the mean motion plays an important role in differentiating one flow from another. Mathematically, the two flows are both governed by the Navier-Stokes (NS) equations, but the different geometric symmetry leads to different simplifications of the equations.

The mean equations of motion for channel flows are

$$\begin{cases} \dfrac{1}{\rho}\dfrac{\partial P}{\partial x} = -\dfrac{d < u'v' >}{dy} + \nu \dfrac{d^2 U}{dy^2} \\ \dfrac{1}{\rho}\dfrac{\partial P}{\partial y} = -\dfrac{d < v'v' >}{dy} \end{cases} \tag{1}$$

Under the assumption of boundary layer, the mean equations of motion for TBL are

$$\begin{cases} \left(U\dfrac{\partial U}{\partial x} + V\dfrac{\partial U}{\partial y} \right) = -\dfrac{d < u'v' >}{dy} + \nu \dfrac{d^2 U}{dy^2} \\ \dfrac{1}{\rho}\dfrac{\partial P}{\partial y} = -\dfrac{d < v'v' >}{dy} \end{cases} \tag{2}$$

A comparison the above equations reveals that the streamwise momentum balance in a channel flow is between the mean pressure gradient and the total shear stress (sum of the mean viscous shear stress and the Reynolds shear stress), while that in TBL is between the mean inertial force and the total shear stress. The mean pressure gradient $\partial P / \partial x$ in channel flow is constant throughout the whole field, while the inertial force $U \partial U / \partial x + V \partial U / \partial y$ in TBL (at a fixed streamwise position) is varying along the wall-normal direction: It is zero at the wall and outside the boundary layer, and peaks somewhere inside the boundary layer (see Figure 1(c)). This observation of the equations suggests that, the wall-normal distribution of the driving force counterbalancing the fluid shear is key to the statistical differences between channel flows and TBL.

The instantaneous streamwise equation of motion for channel flows is

$$\frac{\partial u}{\partial t} + \boldsymbol{u} \cdot \boldsymbol{\nabla} u = -\frac{1}{\rho}\left(\frac{\partial P}{\partial x} + \frac{\partial p'}{\partial x} \right) + \nu \Delta u \tag{3}$$

We define the driving force in TBL (at a given Reynolds number) as the mean inertial force

$$F_x = -\left(U\frac{\partial U}{\partial x} + V\frac{\partial U}{\partial y} \right) = U\frac{\partial V}{\partial y} - V\frac{\partial U}{\partial y} \tag{4}$$

and use it in place of the mean pressure gradient term in Equation 3, i.e.

$$\frac{\partial u}{\partial t} + \boldsymbol{u} \cdot \boldsymbol{\nabla} u = F_x - \frac{1}{\rho}\frac{\partial p'}{\partial x} + \nu \Delta u \tag{5}$$

Simulating Equation 5 with open-channel configuration, applying streamwise periodic boundary conditions, the mean momentum balance in TBL at this Reynolds number should be recovered. We term such a streamwise equilibrium turbulent flow as the equivalent boundary layer (EBL).

2.2 DRIVING FORCE

Before simulating EBL, the wall-normal distribution of the driving force needs to be known. Equation 2 shows the driving force (mean inertial force) to be balanced with the wall-normal derivative of the total shear stress under the boundary layer assumption. Therefore, we consider modeling the total shear stress. Figure 1(a) shows the wall-normal distributions of the total shear stress of TBL at various Reynolds numbers. It can be seen that the total shear stress is Reynolds-number-independent if scaled by the wall shear stress τ_w and the boundary layer thickness δ. Since the driving force is equal to the wall-normal derivative of the total shear stress, it can be scaled by τ_w / δ and δ, as in Figure 1(c). Researches have attempted to model the total shear stress provided its universality. Chen & She (2016) modelled the total shear stress in TBL as

$$\tau_{tot}^+(\eta) = 1 - \eta^{3/2} \tag{6}$$

Kumar & Krishnan (2021) argued that the total shear stress is function of the shape factor H and normalized mean wall-normal velocity V/V_∞, where V/V_∞ is universal (Wei & Klewicki, 2016) while H slowly varies with the Reynolds number. They proposed a model in the form of

$$\tau_{tot}^+(\eta) = H(1 - \frac{V}{V_\infty}) + (H-1)(\eta - 1) \tag{7}$$

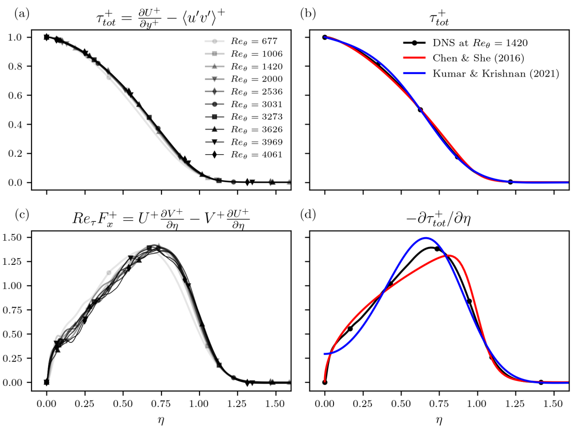

Figure 1. Total shear stress and driving force in TBL. (a) Total shear stress in TBL, from DNS (Schlatter & Örlü, 2010) of TBL at $Re_\theta = 677-4061$; (b) Models (Chen & She, 2016; Kumar & Krishnan, 2021) of TBL total shear stress; (c) Mean inertial force in TBL, equal to the driving force in EBL (legends as in panel a); (d) Driving force obtained from total stress models (legends as in panel b).

where the universal function V/V_∞ can be fitted by a hyperbolic tangent function $V/V_\infty = \tanh(a\eta + b\eta^3)$, with the fitting parameters chosen as $a = 0.5055, b = 1.156$. The above two models are not bounded when $\eta \to \infty$, so in practice η is replaced by a rescaled wall-normal coordinate

$$\bar{\eta} = \frac{\eta}{(1+\eta^\alpha)^{1/\alpha}} \tag{8}$$

This rescaled wall-normal coordinate satisfies $\bar{\eta} \approx \eta$ when η is small, and $\bar{\eta} \to 1$ when $\eta \to \infty$. The parameter α in the function controls the damping rate, and the values fitting the DNS data best are $\alpha = 17$ for the Chen & She (2016) model and $\alpha = 8$ for the Kumar & Krishnan (2021) model.

Figure 1(b,d) shows the modelled total shear stress and its derivative at $Re_\theta = 1420$. The models both agree well with the DNS data in terms of the total shear stress, but the errors are magnified after taking the derivative. The model of Chen & She (2016) behaves well near the wall, but shows a need for higher-order approximations at the edge of boundary layer. The model of Kumar & Krishnan (2021) agrees better with the DNS data in the outer region, but violates $(\partial \tau_{tot}/\partial y)_w = 0$ at the wall, which is obvious since the derivative of Equation 7, $\partial \tau^+_{tot}/\partial \eta = H\left[1-(a+3b\eta^2)/\cosh(a\eta+b\eta^3)\right]-1$ does not reach zero for $\eta = 0$. In sum, errors in the driving force must be induced by taking derivative of the modelled total shear stress. But as volume force, the driving force's integral properties is more important, while the errors in its specific distribution have only secondary influences. This will be confirmed by numerical simulations in Section 3.1.

3 NUMERICAL TESTS

In this section DNS will be carried out to examine the EBL model and to evaluate its performance in generating inflow boundary conditions for TBL. The numerical schemes are described as follows. The second-order central difference and the Crank-Nicolson schemes are used for spatial and temporal discretization respectively. The projection method proposed by Kim *et al.* (2002) is used to decouple the momentum and continuity equations. This projection method ensures the second-order precision in both space and time, and moreover, it requires no pressure boundary condition because the divergence-free condition is handled directly by the 'projection' step. For details of the algorithm the readers are referred to the original papers (Perot, 1993; Kim *et al.*, 2002).

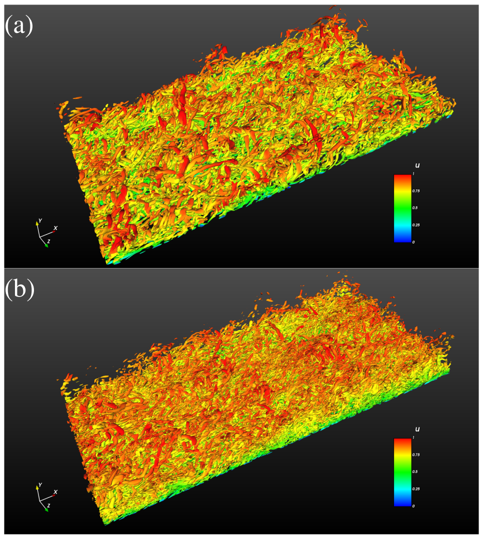

Figure 2. Instantaneous flow fields of EBL. (a) EBL-1000; (b) EBL-2000. Visualized are iso-surfaces of $Q \equiv -0.5(\partial u_i/\partial x_j)(\partial u_j/\partial x_i)$ at $Q = 1$, colored by the streamwise velocity u.

3.1 Simulation of EBL

DNS is carried out for EBL at three Reynolds numbers. The dimensionless governing equations are

$$\begin{cases} \dfrac{\partial \boldsymbol{u}}{\partial t} + \boldsymbol{u}\cdot\nabla\boldsymbol{u} = -\nabla p + \dfrac{1}{Re}\Delta\boldsymbol{u} + \dfrac{1}{2}C_f Re_\tau F^+_x \boldsymbol{e}_1 \\ \nabla\cdot\boldsymbol{u} = 0 \end{cases} \tag{9}$$

The boundary conditions of open-channel are applied, namely periodic boundary conditions for the streamwise and spanwise directions, no-slip wall boundary condition on the bottom, and free-slip boundary condition ($\partial u/\partial y = \partial w/\partial y = 0, v = 0$) on the top. The parameters of the cases are listed in Table 1. The domain sizes are chosen in consideration of the size of VLSM (about $1-2\delta$ wide and $O(10\delta)$ long (Smits *et al.*, 2011)). The grid resolution is chosen to be higher than that used in the DNS research by Schlatter *et al.* (2009). The grid points are stretched following a hyperbolic tangent distribution in the wall-normal direction. The cases EBL-1000, EBL-1420 and EBL-2000 are preliminary examinations of EBL, in which we wish to exclude the influence related to error in the driving forces, so C_f and $Re_\tau F^+_x$ appearing in the expression of driving force are interpolated from the DNS results by Schlatter & Örlü (2010), which are deemed exact. Other than that, we test the performances of driving force models in EBL simulations through cases EBL-1420-KK21 (using Equation 7) and EBL-1420-CS16 (using Equation 6). These two cases have the same configurations to case EBL-1420, except for the driving force.

Figure 2 visualizes the instantaneous flow fields of EBL-1000 and EBL-2000. It is evident that the flow fields are populated by vortical structures typical to wall turbulence. The

Table 1. Parameters of the EBL cases. The case names are numbered by Re_θ of their corresponding TBLs. The last two cases are labelled by their driving force models ('KK21' (Kumar & Krishnan, 2021) and 'CS16' (Chen & She, 2016)). The U_∞, δ involved in the parameters (e.g. the Reynolds numbers and domain sizes) are all based on their nominal values. Δy_e^+ represents the inner-scaled wall-normal grid interval at the edge ($y = \delta$) of the boundary layer.

Case name	Re	Re_τ	L_x, L_y, L_z	N_x, N_y, N_z	$\Delta x^+, \Delta y^+_{min}, \Delta y^+_e, \Delta z^+$
EBL-1000	7783	359	$(8,6,5)\delta$	385, 325, 385	7.5, 0.14, 6.6, 4.7
EBL-1420	11168	492	$(8,4,4)\delta$	385, 325, 385	10.3, 0.10, 9.1, 5.1
EBL-2000	15954	671	$(8,4,4)\delta$	513, 433, 513	10.5, 0.07, 9.9, 5.2
EBL-1420-KK21	11168	492	$(8,4,4)\delta$	385, 325, 385	10.3, 0.10, 9.1, 5.1
EBL-1420-CS16	11168	492	$(8,4,4)\delta$	385, 325, 385	10.3, 0.10, 9.1, 5.1

structures have smaller scales near the wall, and becomes larger further away from the wall. The vortices show streaky patterns, and the spanwise scale of these streaks is about one boundary layer thickness estimated from Figure 2(a). Similar to that reported by Jiménez *et al.* (2010), no ordered hairpin 'forest' as described by Wu & Moin (2009) can be observed in the present visualization. This is probably because the fully developed periodic flow in EBL has lost any transitional effect. A comparison of Figure 2(a) and (b) shows that more finer-scaled structures emerge as the Reynolds number gets higher.

The quantitative characteristics of EBL flow fields are inspected. The first- and second-order statistics of EBL are shown in Figure 3, and compared with the authentic TBL and channel flows at similar Reynolds numbers. It is found in Figure 3(a) that the mean velocity profiles of EBL and TBL agree well under $y^+ = 100$ scaled by inner units. In the wake region, the mean velocity of TBL is higher than that of channel. This is because the high-speed potential flow in the intermittent region injects momentum to the boundary layer (Jiménez *et al.*, 2010). Though the wake of EBL is also higher than that of channel, it is lower than that of TBL, leading to a more distinct discrepancy: the velocity of potential flow in EBL does not reach that of TBL ($U|_{y\gg\delta} = U_\infty$), but stays around $U|_{y\gg\delta} \approx 0.92U_\infty$. The reason for such a discrepancy is still not clear, but it is suspected to be the top boundary condition and the lack of mean wall-normal velocity. The streamwise fluctuation of TBL does not differ much from that of channel, but the spanwise and wall-normal fluctuations and Reynolds shear stress in TBL are significantly higher than that in channel, as shown in Figure 3(b,d). Note that the Re_τ of the channel flow (CHN-540) shown in Figure 3 is about 50 higher than that of the TBL (REF-1420), but this is not the reason for the differences in their statistics. Since the fluctuation intensity of wall turbulence grows with Re_τ increasing, the two kinds of flows would differ even more if they had the same Re_τ. The above observations are consistent with that by Jiménez *et al.* (2010). For statistics which differentiate TBL from channel, our EBL model manages to give results that are closer to TBL. Therefore, though periodic open-channel model is used, the driving force applied succeeds in recovering the characteristics of turbulent fluctuations in authentic TBL.

Pressure and vorticity fluctuations, and high-order statistics of velocity fluctuations, are also checked, as shown in Figure 4. Pressure fluctuations in TBL are different from that in channels throughout the boundary layer. Vorticity fluctuations are also different near the wall. The EBL results are all closer to TBL for these quantities. Figure 4(c) and (d) show the third- and forth-order moments of the streamwise fluctuation. Since the DNS data of channel flows available from literature do not

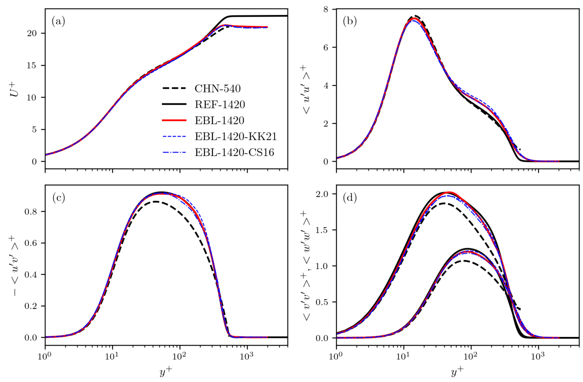

Figure 3. First- and second-order statistics of EBL. (a) Mean streamwise velocity profile; (b) Streamwise fluctuation intensity; (c) Reynolds shear stress; (d) Spanwise (upper cluster) and wall-normal (lower cluster) fluctuation intensities. Black dashed lines (CHN-540) represent channel flow (Lee & Moser, 2015) at $Re_\tau = 543$. Black solid lines (REF-1420) represent authentic TBL (Schlatter & Örlü, 2010) at $Re_\theta = 1420$, i.e. $Re_\tau = 492$. Red and blue lines represent results of the current simulations.

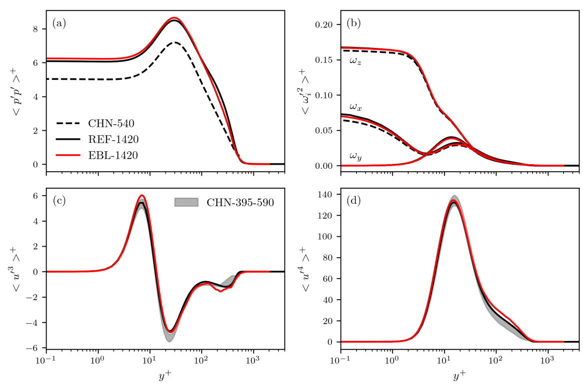

Figure 4. Fluctuations of pressure and vorticity, and high-order statistics of the streamwise fluctuation. (a) Pressure fluctuation intensity; (b) Vorticity fluctuation intensity; (c) Third-order moment of the streamwise fluctuation; (d) Forth-order moment of the streamwise fluctuation. The legends in panel (a) have the same meanings to that in Figure 3. The grey band (CHN-395-590) in panels (c) and (d) represent channel flows (Moser *et al.*, 1999) within $Re_\tau = 395 - 590$.

directly correspond to the Reynolds number of EBL, we take the channel flow statistics within a small range of Reynolds numbers around the target one. The high-order moments of streamwise fluctuations are not significantly different for the channel and TBL, while they are also reasonably captured by the EBL. These results further confirms that the fluctuations in authentic TBL can be correctly represented by EBL.

Also demonstrated in Figure 3 is that EBL gives similar results using either accurate or modelled driving force. The models of Kumar & Krishnan (2021) and Chen & She (2016) perform nearly identically, but the model of Chen & She (2016) has a simpler form. The model of Kumar & Krishnan (2021) contains the shape factor H slowly varying with the Reynolds number. Whether the introduction of such a term improves the model performance at higher Reynolds numbers is not clear, but judging from the Reynolds number range ($Re_\theta < 4000$) covered in Figure 1, the Reynolds-number-independence of driving forces is a fairly good approximation. Moreover, even if the modelled driving force differs from the accurate one (see Figure 1(d)), consistent results can be obtained. This means that EBL is not sensitive the specific distribution of the driving force, as long as its integral characteristic, i.e. the total shear stress (especially on the wall), is correct.

3.2 Simulation of TBL

In order to verify the effectiveness of EBL in generating inflow boundary conditions, DNS of TBL at various Reynolds numbers are carried out using auxiliary simulations of EBL to supply inflow boundary conditions in real time. The governing equations for the main simulation are the N-S equations non-dimensionalized by ρ, U_∞ and the boundary layer thickness at the inlet, δ_{in}.

$$\begin{cases} \dfrac{\partial \boldsymbol{u}}{\partial t} + \boldsymbol{u}\cdot\nabla\boldsymbol{u} = -\nabla p + \dfrac{1}{Re}\Delta\boldsymbol{u} \\ \nabla\cdot\boldsymbol{u} = 0 \end{cases} \tag{10}$$

Periodic boundary conditions are applied to the spanwise direction, no-slip wall boundary conditions are applied to the bottom, far-field boundary conditions ($u = U_\infty$, $\partial v/\partial y = \partial w/\partial y = 0$) are applied to the top, and convective boundary conditions with boundary layer development considered are applied to the outlet. The inflow boundary conditions are decomposed into the mean and fluctuation parts. The prescription of the mean velocity at the inlet is less challenging, and empirical laws or interpolation from existing experimental/numerical data will suffice (Wu, 2017). The mean streamwise and wall-normal velocity used in the present study are interpolated from DNS data of TBL in the public database (Schlatter & Örlü, 2010). The velocity fluctuations at the inlet are extracted from the auxiliary simulation of EBL. The parameters of TBL cases are summarized in Table 2.

In order to validate the simulation results of TBL, the streamwise developing statistics are examined. The three TBL simulation cases cover Reynolds number ranges overlapping each other, so their statistics varying with Re_θ are plotted in Figure 5. Figure 5(a,b) show the friction coefficients and shape factors. Their agreement with results in the literature demonstrates the correctness of the computation. Figure 5(c) compares the variation of Re_τ with Re_θ with the analytic prediction $Re_\tau = Re_\theta/3.27$ proposed by Chen & She (2016). The slopes of the present results are very close to 3.27 in the prediction expression, but the intersection shows a bias of 70.

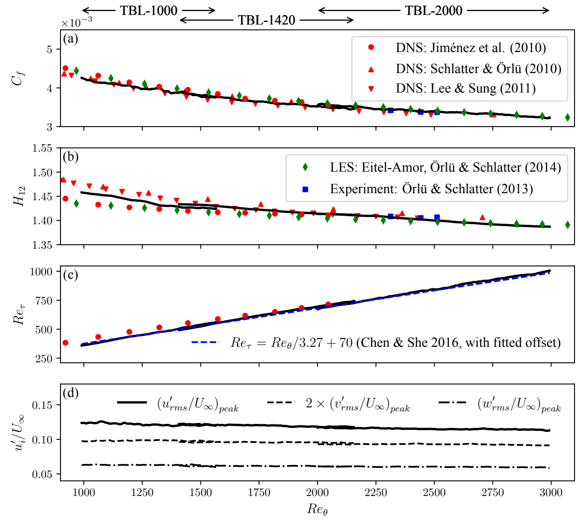

Figure 5. Streamwise developing statistics of TBL. (a) Friction coefficients; (b) Shape factor $H_{12} = \delta^*/\theta$; (c) Friction Reynolds number; (d) Peak values of velocity fluctuations.

Nevertheless, the prediction expression by Chen & She (2016) is based on data of a quite large Reynolds numbers range ($Re_\tau \approx 300-20000$), and when $Re_\tau > 7000$, the bias 70 here leads to a relative error of merely 1%, which is acceptable. Figure 5(d) shows the peaks of fluctuation intensity of three velocity components. As the Reynolds number gets higher, the peaks have lower values and are closer to the wall, scaled in outer units (δ, U_∞).

Notably, the inflow turbulence generated by the EBL proposed by the present study has excellent performance. The statistics of each TBL simulation agree well with the reference data, and follow a natural trend of development from the very beginning of the streamwise domain. Though minor differences and jumps are present, they are all within the scatter of the reference data, especially those DNS data points that are deemed the most precise among researches on TBL. As mentioned in Section 1, the rescaling-recycling based LWS method commonly set the recycling plane $O(10\delta_{in})$ downstream of the inlet in order to skip the unphysical adjustment region. But the further the recycling plane is away from the inlet, the longer the adjustment region will be. Simens *et al.* (2009) measured the adjustment region to be $300\theta_{in}$ long by the peak values of fluctuation intensities of three velocity components. In contrast, these quantities are plotted in Figure 5(d), and no distinct adjustment can be observed. In sum, the inflow turbulence generation by EBL is advantageous in that almost no adjustment region is introduced, and since the computation of EBL is completely independent of the main simulation, it is not affected by the feedback of the error in the main simulation.

To further validate the simulation results near the inlet of TBL simulations, particular streamwise locations are examined. The statistics near the inlets of the three TBL cases are plotted in Figure 6. Because the streamwise locations are very near to the inlets, they can be considered to have the same Reynolds number as the inlets', that is, $Re_\theta = 1000, 1420$ and 2000 for the three cases, respectively. As reference, the DNS results of Schlatter & Örlü (2010) at the same Reynolds numbers are plotted in the figure. The mean velocity profiles of the present simulations are found to agree with the reference even very close to the inlet, and though some errors exist for the streamwise fluctuation intensities, they are of fairly small

Table 2. Parameters of the TBL cases. The case names are numbered by Re_θ at the inlet. Δy_e^+ represents the inner-scaled wall-normal grid interval at the edge ($y = \delta$) of the boundary layer.

Case name	Auxiliary simulation	Re_{in}	Re_θ	Re_τ	Growth (δ_{out}/δ_{in})	$\frac{L_x}{\delta_{in}}, \frac{L_y}{\delta_{in}}, \frac{L_z}{\delta_{in}}$	N_x, N_y, N_z	$\Delta x^+, \Delta y_{min}^+, \Delta y_e^+, \Delta z^+$ (at inlet)
TBL-1000	EBL-1000	7783	$1000 \sim 1540$	$359 \sim 540$	1.61	$36, 8, 5$	$1945, 433, 385$	6.6, 0.14, 5.1, 4.7
TBL-1420	EBL-1420	11168	$1420 \sim 2140$	$492 \sim 720$	1.56	$36, 6, 4$	$1945, 433, 385$	9.1, 0.10, 7.3, 5.1
TBL-2000	EBL-2000	15954	$2000 \sim 2940$	$671 \sim 960$	1.52	$36, 6, 4$	$2305, 513, 513$	10.5, 0.07, 9.0, 5.2

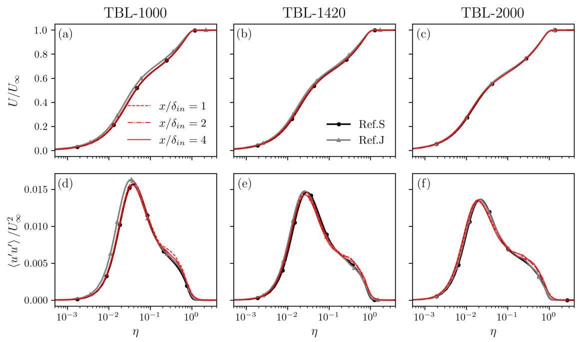

Figure 6. Statistics near the inlets of the present TBL simulation cases. (a,d) Case TBL-1000; (b,e) Case TBL-1420; (c,f) Case TBL-2000. (a-c) Mean streamwise velocity profiles; (d-f) Streamwise fluctuations. The red lines are results at $x/\delta_{in} = 1, 2$ and 4 of each case of the present simulations, and the black and grey lines are DNS results as reference for the inlet ($x = 0$) of each case. Black lines (Ref.S) are from Schlatter & Örlü (2010), and grey lines (Ref.J) are from Jiménez *et al.* (2010).

magnitude. The DNS results of Jiménez *et al.* (2010) using the LWS method are also shown in Figure 6. Note that Reynolds number $Re_\theta = 1000$ for the statistics shown in Figure 6(a,d) actually falls out of the useful range ($Re_\theta = 1100 - 2050$) claimed in their paper. Therefore, evident errors between their results and that of Schlatter & Örlü (2010) are observed in Figure 6(a,d). Such errors are just a downstream effect of the errors in the inflow boundary condition (at $Re_\theta = 620$) generated using the LWS method. In contrast, the inflow turbulence generated using the present EBL are quite accurate at the inlet, hence leading to correct results even close downstream. Judging from the mean velocity, the adjustment region induced by our inflow boundary condition is less than $1\delta_{in}$, if exists at all.

4 Concluding remarks

The present study proposes a new method to generate TBL-type inflow turbulence, namely the EBL. It is based on the open-channel model, applying driving force to recover the mean momentum balance in TBL, and thus fixes the error in approximating TBL by open-channel. EBL is homogeneous in the streamwise direction, so the periodic boundary condition can be applied, overcoming the complexity and arbitrariness of the LWS method.

REFERENCES

Chen, Xi & She, Zhen-Su 2016 Analytic prediction for planar turbulent boundary layers. *Science China Physics, Mechanics & Astronomy* **59** (11).

Jiménez, Javier, Hoyas, Sergio, Simens, Mark P & Mizuno, Yoshinori 2010 Turbulent boundary layers and channels at moderate Reynolds numbers. *Journal of Fluid Mechanics* **657**, 335–360.

Kim, Kyoungyoun, Baek, Seung-Jin & Sung, Hyung Jin 2002 An implicit velocity decoupling procedure for the incompressible Navier–Stokes equations. *International Journal for Numerical Methods in Fluids* **38** (2), 125–138.

Kumar, Praveen & Krishnan, Mahesh 2021 Simple model for mean stress in turbulent boundary layers. *Physical Review Fluids* **6** (2), 24603.

Lee, Myoungkyu & Moser, Robert D. 2015 Direct numerical simulation of turbulent channel flow up to $Re_\tau \approx 5200$. *Journal of Fluid Mechanics* **774**, 395–415.

Lund, Thomas S., Wu, Xiaohua & Squires, Kyle D. 1998 Generation of Turbulent Inflow Data for Spatially-Developing Boundary Layer Simulations. *Journal of Computational Physics* **140**, 233–258.

Moser, Robert D., Kim, John & Mansour, Nagi N. 1999 Direct numerical simulation of turbulent channel flow up to Reτ=590. *Physics of Fluids* **11** (4), 943–945.

Perot, J Blair 1993 An Analysis of the Fractional Step Method. *Journal of Computational Physics* **108** (1), 51–58.

Schlatter, Philipp & Örlü, Ramis 2010 Assessment of direct numerical simulation data of turbulent boundary layers. *Journal of Fluid Mechanics* **659**, 116–126.

Schlatter, Philipp, Örlü, Ramis, Li, Qiang, Brethouwer, Geert, Fransson, J H M, Johansson, A V, Alfredsson, P H & Henningson, Dan S 2009 Turbulent boundary layers up to $Re_\theta = 2500$ studied through simulation and experiment. *Physics of Fluids* **21** (5).

Simens, Mark P, Jiménez, Javier, Hoyas, Sergio & Mizuno, Yoshinori 2009 A high-resolution code for turbulent boundary layers. *Journal of Computational Physics* **228** (11), 4218–4231.

Smits, Alexander J, McKeon, Beverley J & Marusic, Ivan 2011 High–Reynolds Number Wall Turbulence. *Annual Review of Fluid Mechanics* **43** (1), 353–375.

Spalart, Philippe R 1988 Direct simulation of a turbulent boundary layer up to $R_\theta = 1410$. *Journal of Fluid Mechanics* **187**, 37.

Wei, Tie & Klewicki, Joseph 2016 Scaling properties of the mean wall-normal velocity in zero-pressure-gradient boundary layers. *Physical Review Fluids* **1** (8), 1–8.

Wu, Xiaohua 2017 Inflow Turbulence Generation Methods. *Annual Review of Fluid Mechanics* **49** (1), 23–49.

Wu, Xiaohua & Moin, Parviz 2009 Direct numerical simulation of turbulence in a nominally zero-pressure-gradient flat-plate boundary layer. *Journal of Fluid Mechanics* **630**, 5–41.